

Electron focusing in Ag and W single crystals

J. Heil, M. Primke, A. Böhm, and P. Wyder

Hochfeld-Magnetlabor, Max-Planck-Institut für Festkörperforschung and Centre National de la Recherche Scientifique, Boîte Postale 166, 25 Avenue des Martyrs, F-38042 Grenoble Cedex 9, France

B. Wolf

Physikalisches Institut der Universität, Robert-Mayer-Straße 2-4, D-65054 Frankfurt, Germany

J. Major

Max-Planck-Institut für Metallforschung, Institut für Physik, Heisenbergstraße 1, D-70569 Stuttgart, Germany, and Universität Stuttgart, Institut für Theoretische und Angewandte Physik, Pfaffenwaldring 57, D-70569 Stuttgart, Germany

P. Keppler

Max-Planck-Institut für Metallforschung, Institut für Physik, Heisenbergstraße 1, D-70569 Stuttgart, Germany

(Received 14 March 1996)

The nearly ballistic propagation of electrons in Ag and of holes in W is investigated in real space. The carriers are excited by the illumination of a small area on one surface of the sample, and are detected on the opposite side by a Cu point contact. So-called caustics, singularities of the carrier flux in real space related to regions on the surfaces of constant energy in momentum space with zero Gaussian curvature, have been observed. These experiments will permit evaluation of Fermi-surface models and band-structure calculations near the Fermi level. [S0163-1829(96)50828-3]

In very pure metal crystals, the electronic mean free path l^* acquires values in the mm range at low temperatures, $T \leq 4.2$ K. Under these “ballistic” conditions, carriers sent out from a small source ($\ll l^*$) generate a current pattern over some distance $d < l^*$, which is characteristic of the band structure. This behavior has been demonstrated for the semi-metal Bi.¹ Heating realized by the illumination of a small area (hot spot) on one sample surface was used to generate nonequilibrium carriers. A Cu point contact (PC) on the opposite surface, the collector (C), was used for carrier detection. A current enhancement along directions associated with regions of small, yet finite curvature of the constant energy surfaces $S_{E(\mathbf{k})}$ was observed. Here, $E(\mathbf{k})$ is the band structure. If, however, the Gaussian curvature of S_E vanishes completely for some wave vector \mathbf{k} , all group velocities $\mathbf{v}_{\text{gr}} = \hbar^{-1} \nabla_{\mathbf{k}} E(\mathbf{k})$ for neighboring \mathbf{k} states are parallel. This situation generates current singularities in the corresponding \mathbf{v}_{gr} directions. Here $\hbar = h/(2\pi)$, h is Planck’s constant, $\mathbf{v}_{\text{gr}} \perp \mathbf{S}_E$. We call the occurrence of such singularities or caustics electron focusing (EF) in analogy to phonon focusing (PF).² Here we report on the first observation of EF in the noble metal Ag and the transition metal W.

Figure 1(a) shows a scheme of the setup. An Ar-ion laser beam is chopped with a frequency $f \approx 100$ Hz and coupled into an optical fibre. Its end is brought ≈ 20 μm from the sample surface. An area of $(\approx 20$ $\mu\text{m})^2$ is illuminated with a power of ≈ 5 mW. All experiments are performed under liquid ⁴He at $T = 1.5$ K. The EF pattern is recorded by phase-sensitive detection of the voltage V_C between a contact C spot welded to the lower surface and a reference contact R on a sample edge, while the hot spot is scanned across the upper surface by a cryogenic scanner³ (For a homogenous sample, this is equivalent to a fixed hot spot and scanning of

C.) The EF pattern can be interpreted as the far-field radiation pattern of a carrier point source. C is produced by electrochemical etching of a Cu wire of 100 μm diameter. Electron injection by an emitter PC has been successfully used in Bi,⁴ but failed in Ag and W for unknown reasons.

The samples were cut from single crystals by spark erosion to slabs of thickness $d \approx 2$ mm with the surface perpendicular to [110]. The Ag crystals were annealed for 72 h at 800 °C in flowing argon. d was reduced to ≈ 0.5 mm for Ag by electrochemical polishing and to ≈ 0.35 mm for W by etching.⁵ After plasma etching, a constantan (CuNi) layer of ≈ 100 nm thickness was sputtered onto the Ag surface because experiments on Bi had revealed the thermoelectric origin of V_C , and we expected signals orders of magnitude lower for Ag because of its small thermopower. The CuNi film was deposited to create an extended thermocouple to allow injection of carriers at specific positions by local heating. No film was deposited onto the W surface.

Results for Ag are displayed in Figs. 2(a) and 2(b). Despite the image distortions due to an early version of the scanner, two bright electron caustics enclosing a bright field bounded by faint dark borders are clearly visible. They are generated by the states around the necks of the Fermi surface (FS), outlined by the shading in Fig. 1(b). From computed PF patterns, we conclude that no traces of PF (such as were seen in Bi) are visible.¹

Based on a great wealth of available data,⁶ the FS of Ag has been parametrized, and FS models are given as five- or seven-term Fourier sums in \mathbf{k} .⁷⁻⁹ $E(\mathbf{k})$ is available from a Slater-Koster (SK) interpolation scheme based on the LCAO method.¹⁰ To calculate a theoretical EF pattern, the Fermi wave vector \mathbf{k}_F and \mathbf{v}_{gr} are determined for up to 10^7 random \mathbf{k} directions assuming that the fit represents the real $E(\mathbf{k})$

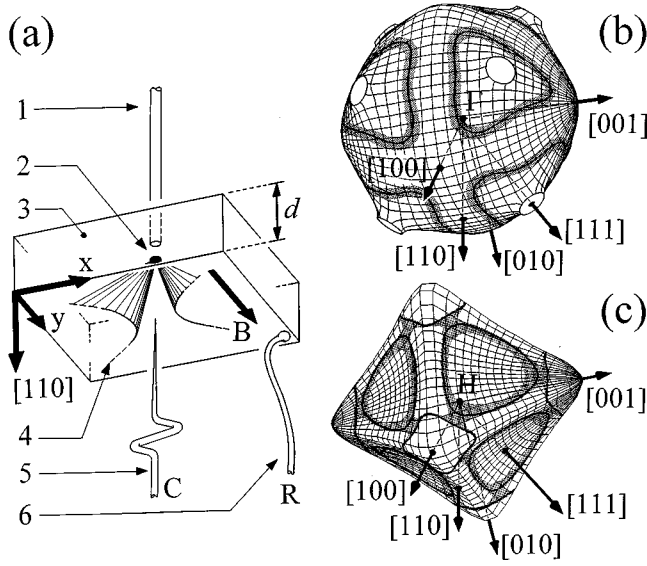


FIG. 1. (a) Scheme of the setup. An optical fiber (1) scans a light spot (2) across the upper (110) surface of the sample (3) of thickness d . The EF pattern (4) on the lower surface is detected by recording the voltage V_C between a collector contact C (5) and a reference contact R (6). A magnetic field \mathbf{B} can be applied in the (110) plane. (b) The electron FS of Ag after Ref. 10. (c) The hole FS of W after Ref. 10. Regions with Gaussian curvature lower than 10^{-21} m^2 in (b) and $2 \times 10^{-21} \text{ m}^2$ in (c) are shaded; the heavy lines show locations with zero Gaussian curvature.

sufficiently well within a narrow energy interval of several $k_B T_h$ around E_F . Here, k_B is Boltzmann's constant, T_h is the temperature of the hot spot, and E_F is the Fermi energy. For each \mathbf{k} , we calculate where \mathbf{v}_{gr} hits the surface and establish a signal proportional to the \mathbf{v}_{gr} component normal to the surface and to $\mathbf{k}_F^2 (\mathbf{k}_F / |\mathbf{k}_F| \cdot \mathbf{v}_{\text{gr}} / |\mathbf{v}_{\text{gr}}|)^{-1}$ (assuring homogeneous sampling in \mathbf{k} space) at this position. These signals are then summed up to give the EF pattern. Figures 2(c), 2(d), and 2(e) show EF patterns computed for the seven-parameter sets from Refs. 7, 8, and 9, respectively, assuming $l^* \rightarrow \infty$ and $V_C \sim j_n$, the current density component normal to the surface. Except for the SK-LCAO fit, $\nabla_{\mathbf{k}} E(\mathbf{k})$ is adjusted at E_F by an additional fit factor. The EF patterns calculated from the five-parameter fits after Refs. 7 and 8, and the fit with the SK-LCAO data¹⁰ are very similar to Fig. 2(e) and thus are not shown here.

A quantitative comparison of experiments and simulations is difficult because of the image distortions introduced by the scanner and by a nonideal sample geometry (no manipulation has been performed on the data). However, Figs. 2(b) and 2(c) can clearly be ruled out. \mathbf{k}_F is claimed to be precise to 10^{-2} , 2×10^{-3} , and 10^{-5} for Refs. 7, 8, and 9, respectively. The EF pattern is obviously sensitive to even these small differences, thus providing a powerful check for the FS geometry. In the following we take the representation of the FS in Ref. 9 to approximate the real $E(\mathbf{k})$, and use it for all calculations for Ag, since its caustics correspond well to those derived with the SK-LCAO data,¹⁰ but it is much easier to handle in numerical calculations.

The ‘‘ballistic’’ analogue of the usual thermal diffusion current is calculated as follows.¹ Electrons in the hot spot are described by the Fermi distribution function f_h for

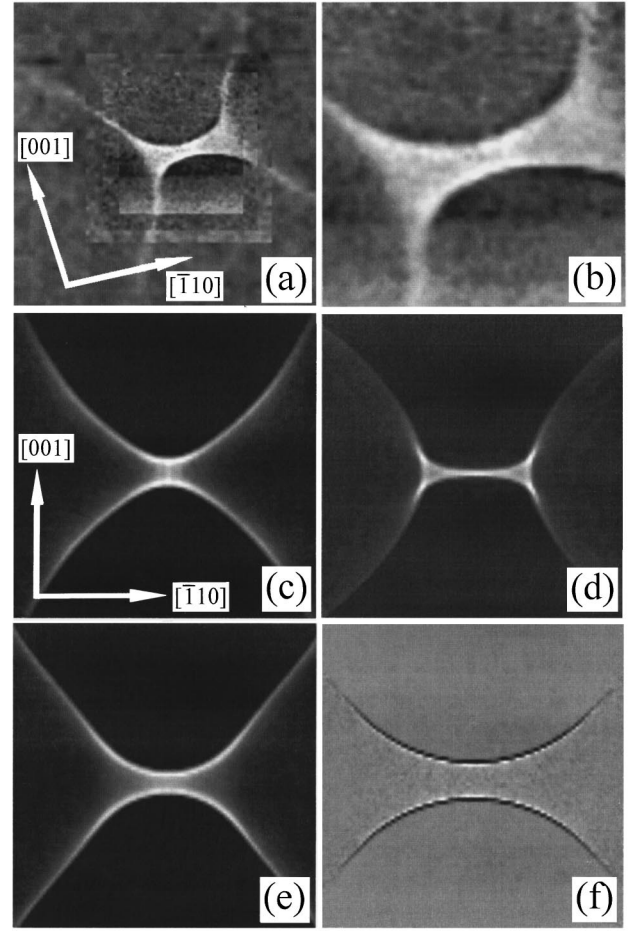


FIG. 2. EF pattern on the (110) surface of Ag. V_C is shown in gray scale as a function of the fiber position. (a) Composite EF pattern, the frames are $\approx (1, 0.6, 0.5, \text{ and } 0.4 \text{ mm})^2$, consisting of $(40, 40, 50, \text{ and } 50)^2$ raw data, respectively. $0 \text{ nV} \leq V_C \leq 2 \text{ nV}$ from black to white. (b) Zoom into the innermost frame of (a). (c–e) EF patterns computed assuming $V_C \sim j_n, l^* \rightarrow \infty$ and that electrons at E_F emerge from a point source. Seven-parameter fits to the FS from Refs. 7, 8, and 9 were used for (c), (d), and (e), respectively. The frames are $(1.5d)^2$. (f) EF pattern computed for thermally excited electrons with the parameters from Ref. 9. The frame is $(0.8d)^2$, corresponding to that of (b).

the high-temperature T_h , those in the bulk are described by f_c at the low temperature T_c , $f_{h,c} = (\exp\{[E - \mu(T_{h,c})] / k_B T_{h,c}\} + 1)^{-1}$. Here, $\mu(T)$ is the chemical potential, the T dependence of which is given by the $E(\mathbf{k})$ used.⁹ Each energy layer generates its own EF pattern $V_C^E(\mathbf{r})$, where \mathbf{r} is the position vector. The total signal is given by $V_C(\mathbf{r}) \sim \int_{-\infty}^{\infty} [f_h - f_c] V_C^E(\mathbf{r}) dE$. The result for $T_h = 100 \text{ K}$ (certainly too high, but chosen to circumvent the problem of small differences of large numbers in the numerical calculations) and $T_c = 1.5 \text{ K}$ is shown in Fig. 2(f). The bright caustics are produced by electrons with $E > E_F$ spreading out from the hot spot. The dark rims stem from electrons at $E < E_F$ moving from occupied states in the bulk into empty states in the hot spot. Since \mathbf{S}_E changes with E , the bright and dark caustics appear at different positions in real space.

The traces in Fig. 3(a) were recorded by scanning the hot spot along the $[001]$ direction across the rims for different magnetic fields $\mathbf{B} \parallel [\bar{1}10]$. Figure 3(b) shows V_C according to

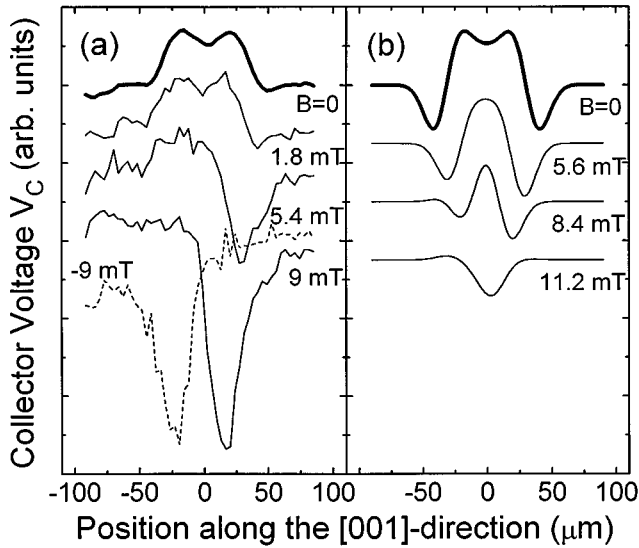


FIG. 3. (a) Central linecuts of an EF pattern along $[001]$ for different values of $\mathbf{B} \parallel [110]$. The traces are averaged over 10 scans covering 50 positions. (b) Collector signal calculated according to our model. For clarity, the curves have been shifted vertically to separate them.

our model; the semiclassical equations of motion were solved for up to 10^5 events using $E(\mathbf{k})$ from Ref. 9. To simulate the hot spot, the data were smoothed with a Gaussian of $20 \mu\text{m}$ width. The general character of the data is reproduced, namely, the occurrence of two bright and dark caustics and their increasing asymmetry with rising \mathbf{B} . However, the model is not quantitatively correct: the intensity of the dark caustics is too high at $\mathbf{B} = \mathbf{0}$, and does not increase with \mathbf{B} as in the experiment.

To include the initially intended effect of the CuNi layer, imagine the thermocurrent flowing through the tiny hot spot from CuNi to Ag, while flowing back through the large cold interface. The voltage will mainly drop at the hot spot if the electrode resistances are neglected. The electrochemical potential difference calculated from the thermopower $S(T)$ of Ag and CuNi implies a net electron current flowing from Ag to CuNi through the hot spot.^{11,12} If included, this current even increases the disagreement with the experiment at $\mathbf{B} = \mathbf{0}$, since it further enhances the dark rims.

A first reason for this discrepancy might be that the electrical contact of the CuNi layer to the Ag sample is bad and the layer only acts as an efficient absorber for light. Control experiments on crystals with clean surfaces, or ones blackened with ink or varnish, failed, probably because most of the light was lost by reflection and also poor thermal coupling of the varnish to the sample. Second, the literature values for S might not apply to our (dirty) sputtered system. In addition, $S_{\text{Ag}}(T < 10 \text{ K})$ is known to exhibit sample-dependent ‘‘giant’’ thermopowers.¹³ The role of the CuNi layer is not yet understood.

If the ‘‘ballistic’’ thermopower of Ag is considered to be the sole source of the EF pattern as in Figs. 2(f) and 3(b), then some process favoring electron transport from T_h to T_c has to be included to improve the agreement with experiment. An energy-dependent scattering time $\tau(E)$ has been proposed to explain the sign of S_{Ag} .¹⁴ This can yield the

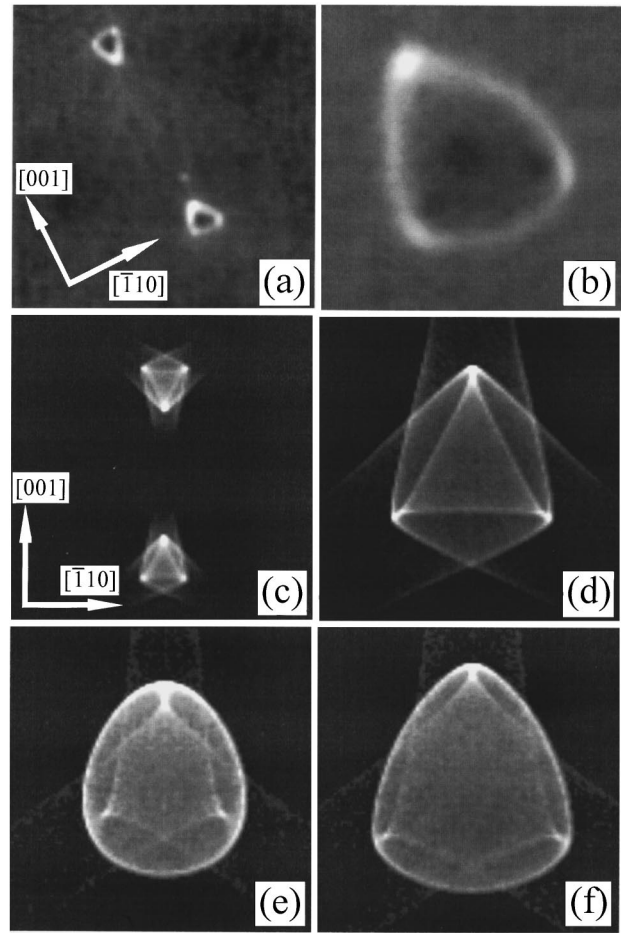


FIG. 4. (a) EF pattern on the (110) surface of W, the frame is $(790 \mu\text{m})^2$, $0 \text{ nV} \leq V_C \leq 1.8 \text{ nV}$, $(80)^2$ raw data. (b) Zoom into (a), the frame is $(140 \mu\text{m})^2$, $-0.4 \text{ nV} \leq V_C \leq 6 \text{ nV}$, $(70)^2$ raw data. (c) EF pattern computed for holes at E_F after Ref. 15, the frame is $(2.5d)^2$. (d) Zoom into (c), the frame is $(0.7d)^2$. (e) Like (d), but with the data from Ref. 10. (f) Like (e), but with E_F lowered by 0.23 eV .

desired behavior. However, we prefer not to go into further detail here, since assumptions about the amount and the nature of scattering would only further increase the amount of ambiguity.

Figures 4(a) and 4(b) show EF patterns recorded on the (110) surface of W; the prominent features are obviously generated by holes from the FS centered at the H point of the Brillouin zone shown in Fig. 1(c). The FS has rounded corners and triangular faces that bend slightly inwards. Two different sets of states with zero Gaussian curvature exist: states on the lines enclosing the concave regions on the triangular faces of the FS produce the bright triangular caustics with the three bright spots at its edges where the $[111]$ direction hits the surface; states around the convex corners generate a series of faint lines connecting the triangles. Several dark spots are visible both inside the triangle, and where the $[100]$ direction hits the surface. They might be due to electrons from the so-called ‘‘electron-jack’’ surface.¹⁵ As in Ag no traces of PF show up.

The EF patterns calculated from an analytical approximation of the hole FS of W for two parameter sets^{15,16} are very similar, thus we display only the result after Ref. 15 in Figs.

4(c) and 4(d). The agreement with Figs. 4(a), and 4(b) is poor, although de Haas–van Alphen data are well described. Figures 4(e) and 4(f) show simulations with $E(\mathbf{k})$ from Ref. 10. Only holes at E_F are taken into account. The general features of the experiment are reproduced. Parameter adjustments (with regard to other FS data) can improve the fits. Just to show the sensitivity of the EF pattern to parameter changes, Fig. 4(f) shows the effect of a decrease of E_F by 0.23 eV, which happens to improve the overall agreement with Fig. 4(b).

In conclusion, we have presented experiments revealing the nearly ballistic transport of carriers excited by illumination in Ag and W. A focusing of carriers (EF) along \mathbf{v}_{gr} -directions belonging to states with zero Gaussian curvature on the FS is clearly demonstrated. Caustics in $V_C(\mathbf{r})$ are clearly visible. Our crude theory assumes two distinct equilibrium distributions of the carriers, one in the heated region and one in the cold crystal, plus completely ballistic carrier propagation. While it reproduces the observed caustics, it

does not describe either the signal intensities, or their dependence on a magnetic field, quantitatively correctly. The spectral composition of the signal, the distribution function of the carriers, and their spatial variation, as well as the details of the transport and the exact way in which the collector PC detects them are not yet well understood. These problems remain a challenge for future work. Once understood, experiments of this kind may shed new light on transport and thermoelectricity; they offer a unique possibility for \mathbf{k} -resolved studies, the electronic dispersion of the medium acting as a spectrometer. It should then be possible to investigate the anisotropy of other quantities, for example, energy gaps at E_F .

We wish to thank A. G. M. Jansen for supplying the Ag samples, P. Strobel for help in annealing the Ag samples, D. A. Papaconstantopoulos for generously making his programs available to us, and J. Bass for carefully reading the manuscript.

-
- ¹J. Heil, M. Primke, K. U. Würz, and P. Wyder, Phys. Rev. Lett. **74**, 146 (1995).
²J. P. Wolfe, Phys. Today **48** (9), 34 (1995).
³J. Heil, A. Böhm, M. Primke, and P. Wyder, Rev. Sci. Instrum. **67** (1), 307 (1996).
⁴M. Primke, J. Heil, and P. Wyder in *Real Space Resolved Investigation of Ballistic Electron Transport in Bi Single Crystals* [Physica B **218**, 26-30 (1996)].
⁵Ag: electrolyte: 50 vol % HNO₃ in H₂O, cathode: stainless steel, $V=2V_{\text{dc}}$, $j\approx 1\text{A}/\text{cm}^2$, room temperature W: two to three parts HF (40%) + one part HNO₃ (65%), room temperature.
⁶A. P. Cracknell, in *Metals: Phonon States, Electron States and Fermi Surfaces*, edited by K. H. Hellwege and J. L. Olsen, Landolt-Börnstein, New Series, Group III, Vol. 13, Pt. c (Springer-Verlag, Berlin, 1984).
⁷D. J. Roaf, Philos. Trans. R. Soc. London Ser. A **255**, 135 (1962).
⁸M. R. Halse, Philos. Trans. R. Soc. London Ser. A **265**, 507 (1969).
⁹B. Bosacchi and P. Franzosi, J. Phys. F **6**, L99 (1976).
¹⁰D. A. Papaconstantopoulos, *Handbook of the Band Structure of Elemental Solids* (Plenum, New York, 1986).
¹¹P. A. Schroeder, R. Wolf, and R. Woolam, Phys. Rev. A **138**, 105 (1965).
¹²J. S. Touger and M. P. Sarachick, Solid State Commun. **20**, 1 (1976).
¹³R. D. Barnard, *Thermoelectricity in Metals and Alloys* (Taylor & Francis, London, 1972).
¹⁴J. M. Ziman, in *The Physics of Metals*, edited by J. M. Ziman (Cambridge University Press, London, 1969), Vol. 1, p. 1.
¹⁵R. F. Girvan, A. V. Gold, and R. A. Phillips, J. Phys. Chem. Solids **29**, 1485 (1968).
¹⁶S. W. Hui and J. A. Rayne, J. Phys. Chem. Solids **33**, 611 (1972).